Porosity of the Marcellus Shale: A contrast matching small-angle neutron
 scattering study

3

Jitendra Bahadur^{1, 2}, Leslie F Ruppert³, Vitaliy Pipich⁴, Richard Sakurovs⁵, Yuri B. Melnichenko^{2†}

¹Solid State Physics Division, Bhabha Atomic Research Centre, Mumbai, 400094, India

²Biology and Soft Matter Division, Oak Ridge National Laboratory, Oak Ridge, TN, USA

³U.S. Geological Survey, MS 956, Reston, VA 20192, USA

⁴Jülich Centre for Neutron Science JCNS-FRM II, Outstation at FRM II, D-85747 Garching, Germany

⁵ The Commonwealth Scientific and Industrial Research Organisation (CSIRO) — Energy, Riverside Life Science Centre, 11 Julius Ave, North Ryde, NSW, 2113, Australia

[†]Deceased March 16, 2016

4

5 Abstract

6

7

8

9

10

11

12

13

14

Neutron scattering techniques were used to determine the effect of mineral matter on the accessibility of water and toluene to pores in the Devonian Marcellus Shale. Three Marcellus Shale samples, representing quartz-rich, clay-rich, and carbonate-rich facies, were examined using contrast matching small-angle neutron scattering (CM-SANS) at ambient pressure and temperature. Contrast matching compositions of H₂O and D₂O and toluene and deuterated toluene were used to probe open and closed pores of these three shale samples. Results show that although the mean pore radius was approximately the same for all three samples, the fractal dimension of the quartz-rich sample was higher than for the clay-rich and carbonate-rich

samples, indicating different pore size distributions among the samples. The number density of pores was highest in the clay-rich sample and lowest in the quartz-rich sample. Contrast matching with water and toluene mixtures shows that the accessibility of pores to water and toluene also varied among the samples. In general, water accessed approximately 70–80% of the larger pores (>80 nm radius) in all three samples. At smaller pore sizes (~5-80 nm radius), the fraction of accessible pores decreases. The lowest accessibility to both fluids is at pore throat size of ~25 nm radius with the quartz-rich sample exhibiting lower accessibility than the clayand carbonate-rich samples. The mechanism for this behaviour is unclear, but because the mineralogy of the three samples varies, it is likely that the inaccessible pores in this size range are associated with organics and not a specific mineral within the samples. At even smaller pore sizes (~<2.5 nm radius), in all samples, the fraction of accessible pores to water increases again to approximately 70–80%. Accessibility to toluene generally follows that of water; however, in the smallest pores (~<2.5 nm radius), accessibility to toluene decreases, especially in the clayrich sample which contains about 30% more closed pores than the quartz- and carbonate-rich samples. Results from this study show that mineralogy of producing intervals within a shale reservoir can affect accessibility of pores to water and toluene and these mineralogic differences may affect hydrocarbon storage and production and hydraulic fracturing characteristics.

1. Introduction

15

16

17

18

19

20

21

22

23

24

25

26

27

28

29

30

31

- 33 Shale is one of the important unconventional gas resources in the U.S., Canada, and the world.
- Production of shale gas in U.S. has increased from 0.75 trillion cubic feet (Tcf) in 2005 to
- approximately 15.8 Tcf in 2016 (U.S. Energy Information Administration, 2012, 2017). In shale,
- oil, gas, and formation water are the fluids that are retained in the rock; however, there are major

uncertainties in how and where the gas is held and how gas production is affected by the percentages of open and closed porosity.

The storage of hydrocarbon gas in organic-rich shale reservoirs occurs in two ways:1) via physisorption of gas molecules in the micropores (≤2.5 nm) and mesopores (>2.5–50 nm) embedded in organic matter and possibly in some clays, 2) compressed gas stored in macropores (>50 nm) and natural fractures, and solution gas in entrained water (Busch and Gensterblum, 2011).

Reservoir rock wettability, the ability of the interstices in rocks to be wet by a fluid, is an important factor in reservoir development as it affects capillary pressure, hydrocarbon migration, hydrofracturing characteristics, and therefore directly influences ultimate recovery (Abdullah et al., 2007). Reservoir rocks are composed of minerals that can be water-wet, oil-wet, or mixed-wet (usage of Abdullah et al., 2007) if they do not have a preference for one fluid over the other. The wettability of a rock is dependent on its mineral matter composition and saturation history. The primary minerals, quartz, clay, and carbonates, within a reservoir rock can have differing wetting characteristics if they had been in contact with oil, even though they are typically waterwet in their native form (Abdullah et al., 2007).

Understanding shale pore structure is therefore one of the keys to understanding gas storage in these continuous, or unconventional, reservoirs. Various techniques are available for characterizing the porosity in coal and shale. These include gas adsorption, mercury intrusion porosimetry (MIP), transmission electron microscopy (TEM), and small-angle neutron scattering (SANS) techniques. Gas adsorption and MIP techniques do not provide information about inaccessible, or closed, pores and TEM gives only limited information about pore connectivity.

Small-angle X-ray scattering (SAXS) provides information on all pores but it cannot differentiate between accessible and inaccessible pores. Contrast-matching small-angle neutron scattering (CM-SANS) techniques allow for the characterization of both accessible and inaccessible pores as a function of pore size. CM-SANS was originally utilized to investigate closed porosity in a variety of materials including polymer resins (Foster and Jensen, 1990), coal char (Brumberger and Goodisman, 1983), and vapour-deposited metal alloys (Hall et al., 1996). More recently, Melnichenko et al. (2012) used high pressure supercritical CO₂ and deuterated methane (CD₄) for CM-SANS experiments on coal for the determination of accessible and inaccessible porosity. Others have used this technique to examine microporous carbon (Bahadur et al., 2015a); coal (Coetzee et al., 2015; He et al., 2012; Mastalerz et al., 2012; Melnichenko et al., 2012; Radlinski and Mastalerz; Radlinski et al., 2004; Sakurovs et al., 2012; Sakurovs et al.; Staib et al., 2013; Zhang et al., 2015), and shale (Bahadur et al., 2014; Bahadur et al.; Blach et al.; Clarkson et al., 2012; Clarkson et al., 2013; Furmann et al., 2014; Gu et al., 2015; Gu et al., 2016; Mastalerz et al., 2012; Ruppert et al., 2013). A comprehensive overview of CM-SANS technique has been provided by Melnichenko (2016, chapter 10 and references within). In geologic materials the scattering is largely from density fluctuations in the mesoscopic (µmnm) length scale, and in porous materials the greatest density contrasts are usually between pores and matrix (Radlinski, 2006). SANS profiles provide information on the total porosity and pore size distribution within a sample The scattering intensity is also proportional to the square of the difference in scattering length density (SLD) between the solid and the pores. Scattering length densities of materials are determined by its density and chemical composition. Additional background can be found in Bahadur et al. (2015a) and Melnichenko (2016).

59

60

61

62

63

64

65

66

67

68

69

70

71

72

73

74

75

76

77

78

79

The CM-SANS technique requires two separate measurements on an individual sample. The first measurement records the scattering from the sample at vacuum on a dry sample and provides the scattering that arises from density contrast between the solid matrix and all of the pores. The second measurement utilizes a wetting fluid, which can be a pressurized gas or a liquid that has a similar SLD to the solid matrix (includes all components within the sample including mineral matter and organic material). This fluid fills the accessible pores, thus eliminating all of the scattering contribution from open pores; any remaining scattering comes from the inaccessible pores that the fluid cannot penetrate. The ratio of the scattering intensity from the sample with the fluid present to that from the sample in a vacuum provides information on the fraction of pores that is inaccessible to the fluid (Melnichenko et al., 2012; Radlinski et al., 2000).

A pore may be inaccessible to a fluid because it is physically closed or because the pore surface is non-wettable to a given fluid due to the surface tension of the fluid. If the latter, the same pore may be accessible to a different fluid that does wet the pore surface. Variation in the fraction of inaccessible pores in a sample using different fluids indicates that there are differences in the wettability of pore surfaces within the sample, assuming that the size of the pore throats examined are larger than the size of the fluid molecule (László et al., 2012; Utpalendu et al., 2014). Deuterated fluids can have high SLD values, making them convenient contrast matching fluids. In this study we use a mixture of protonated and deuterated liquids including water (H₂O) and d-water (D₂O) and toluene (C₇H₈) and d-toluene (C₇D₈). By comparing the fraction of inaccessible pores as determined by water penetration with that by toluene penetration, the comparative wettability of minerals and organic material in shale can be determined on a length scale of tens to hundreds of nanometres.

Although there have been studies on wettability of unconventional petroleum reservoirs rocks (Gao and Hu, 2015; Xu and Dehghanpour, 2014), we know of no studies that examine the role of CM fluids on the wettability of both accessible and inaccessible pores in low permeable reservoir rocks. In this work, our aim is to examine the role of CM fluids on the determination of accessible and inaccessible porosity in samples of the Marcellus Shale.

2. Geology of the Marcellus Shale

103

104

105

106

107

108

109

110

111

112

113

114

115

116

117

118

119

120

121

122

123

124

125

The Middle Devonian Marcellus Shale (Soeder et al., 2014), which averages 30.8 m thick, extends over 80,000 km² in southernmost Ontario, southern New York, western and northern Pennsylvania, most of West Virginia, parts of west central Virginia, and eastern Ohio within the Appalachian Plateaus Physiographic Province (Fig. 1) in the central Appalachian basin, U.S.A. The Marcellus Shale was deposited in an anoxic shallow interior sea on a westward prograding clastic wedge that was later overlain by coarse-grained Upper Devonian clastic sediments of the Catskill Delta (Milici and Swezey, 2014; Soeder et al., 2014). Based on 2-D models, the original depth of burial was >3.7 km (Rowan, 2006) deeper than the current burial depths of the gas-producing area of the shale (2–3 km) (Milici and Swezey, 2014). In the Appalachian basin the oil window ranges from the Early Devonian in central Ohio to Early Pennsylvanian in west-central Pennsylvania, and the gas window was reached in the Middle Triassic, near the Ohio-West Virginia border (Milici and Swezey, 2014). Lithologically, the formation is complex with interbedded siltstone and mudstone, with minor limestone beds and primary mineral constituents include quartz, clay, carbonate, feldspar, and minor amounts of pyrite and other accessory minerals. Total organic content (TOC) tends to decrease from New York southward to West Virginia (Milici and Swezey, 2014) and ranges from approximately 2– 10% in areas where gas is produced.

Although gas produced from the Marcellus Shale is commonly thought to be dry, associated natural gas liquids are produced from the Marcellus in southwestern Pennsylvania and northwestern West Virginia. The Marcellus Shale was chosen for analysis because this formation, and the underlying Utica Shale, have provided 85% of the U.S. shale gas production growth since 2012 (U.S. Energy Information Agency, 2016).



Figure 1. Extent of Devonian shale in the Appalachian basin. Hatched patterns show the Marcellus Shale extent. Figure modified from paper published by Soeder et al. (2014).

3. Experimental

3.1 Sample Characterization:

Three fresh core sections (Table 1) of the Middle Devonian Marcellus Shale from an exploratory well drilled in West Virginia in the dry gas window were obtained from industry.

The samples were chosen to represent the mineralogy of producing intervals of the Marcellus

Shale – quartz-rich (Mar-1), clay-rich (Mar-2), and carbonate-rich (Mar-3) intervals (Table 1). The length of the core sections ranged from 7.3–17.98 cm (Table 1) and the sections were wrapped in plastic and stored refrigerated until they were slabbed and processed. Each core sample was slabbed (water cooled) from top to bottom perpendicular to bedding, and then ground in a Fritsch Pulverisette 2 mortar grinder. To minimize bias that can be introduced while grinding minerals with different hardnesses, the same pressure, rotation speed, and grinding times were used for all three samples. Following grinding, they were hand sieved to produce 0.5–1.0 mm size particles that were representative of the entire length of the core piece. Representative sub-splits of the sieved particles were oven dried at 100°C overnight before they were measured with SANS. Additional sub-splits were analyzed for: carbon, hydrogen, nitrogen, oxygen, and sulfur (CHNOS) analyses, total organic carbon (TOC), and quantitative x-ray diffraction.

Table 1 Semi-quantitative mineralogy of Marcellus Shale samples. Scattering length density (SLD) was calculated using the volume averaged SLDs from the mineralogical composition of the samples (Bahadur et al, 2014). The uncertainty of the semi-quantitative XRD analysis is $\pm 5\%$ (Hosterman and Dulong, 1989).

Sample Number	Sample Length (cm)	Depth (m)	Quartz (%)	Calcite (%)	Illite (%)	Pyrite (%)	Calculated sample SLD (10 ¹⁰ cm ⁻²)
Mar-1	7.3	2302.2	66	4	23	7	4.01
Mar-2	17.98	2306.8	51	9	34	7	3.99
Mar-3	7.3	2310.2	37	35	20	8	4.18
Mineral SLD (10 ¹⁰ cm ⁻²)			4.2	4.7	3.4	3.8	

Table 2 Carbon, hydrogen, nitrogen, oxygen, sulfur, total organic carbon contents (TOC), reported in weight percent, and calculated H/C and O/C ratios of the Marcellus Shale samples.

Sample	C wt.%	H wt.%	N wt.%	O wt.%	S wt.%	TOC wt.%	Atomic H/C	Atomic O/C
Mar-1	6.69	0.78	0.24	4.31	3.84	5.64	1.38	0.46
Mar-2	10.73	0.91	0.38	5.05	3.79	9.60	1.01	0.36
Mar-3	8.09	0.77	0.28	11.37	3.54	4.54	1.19	1.06

3.2 SANS experiments

SANS measurements were carried out on the KWS-1 and KWS-3 instruments at the FRM-II reactor, Germany. The KWS-1 (Heinz Maier-Leibnitz Zentrum, 2015a) is a conventional pinhole based SANS instrument with an available Q-range of Q=0.0007–0.5 Å⁻¹, where Q (= $4\pi sin\theta/\lambda$, 20 is the scattering angle, λ is the wavelength of the neutron) is the scattering vector. For this study the Q-range of ~0.002–0.3 Å⁻¹ was investigated. An approximate relationship between the scattering vector Q and the pore radius r, (r \cong 2.5/Q) has been used to relate the length scales in the reciprocal and real space (Radlinski et al., 2000). In order to access smaller Q values (corresponding to larger pores), measurements were also carried out on the KWS-3 (Heinz Maier-Leibnitz Zentrum, 2015b), a very small angle neutron scattering (VSANS) instrument which operates on the focussing mirror principle. The sample to detector distance was kept at 9.5 m which allowed us to access the Q-range of ~0.0001–0.003 Å⁻¹. The sieved Marcellus Shale particles were loaded into 1 mm path length quartz cuvettes for measurement. Following measurement of the dry samples, mixtures of H₂O/D₂O (water/d-water) and C₇H₈/C₇D₈ (toluene/d-toluene) of different SLDs were prepared. The SLD of the mixtures was

varied from $\sim 1 \times 10^{10}$ to 5×10^{10} cm⁻² by changing the volume fraction of the deuterated to protonated components from ~ 0 to 80% to match the SLD of the samples. The liquid mixtures were added to the sub-splits of the three powder samples approximately 1 hour prior to SANS analysis. SANS measurements on both dry and wet samples were performed under ambient conditions. The weight of powder samples during SANS measurement was estimated by subtracting the weight of empty cuvette from that of powder filled cuvette. The variation in the sample mass/packing density during one set of contrast matching experiments was within 8%. Figure 2 shows the volume fraction of deuterated components and corresponding SLD of H_2O/D_2O and toluene/d-toluene mixtures chosen for contrast variation SANS measurements. It was observed that scattering profiles below $Q\sim 10^{-3}$ Å⁻¹ (equivalent to pore radii of 250 nm) deviate from power law behaviour mainly due to multiple scattering. The analysis of the data was carried out for $Q>10^{-3}$ Å⁻¹ to avoid the effects of multiple scattering.

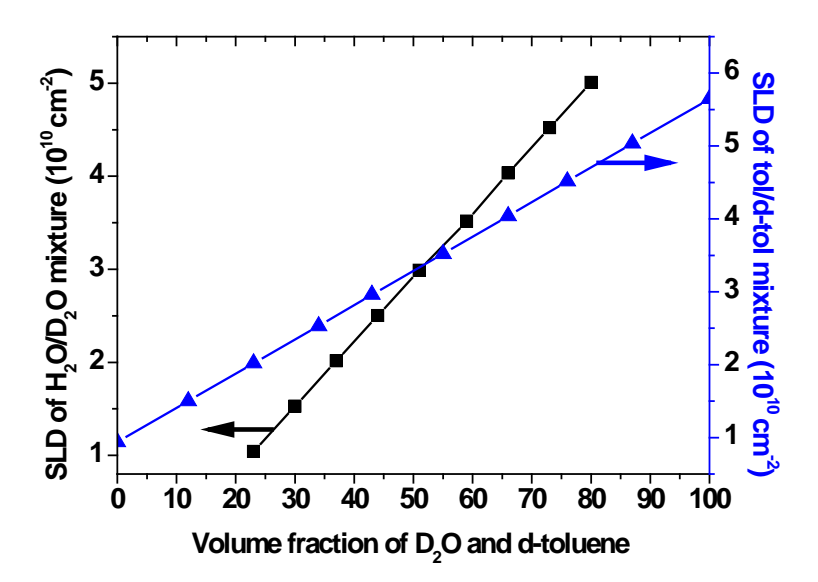


Figure 2. Scattering length density (SLD) variation of water/d-water (H_2O/D_2O) and toluene/d-toluene (tol/d-tol) mixtures as a function of deuterated volume fractions. Arrows point to the respective y axis for water and toluene.

Because the relatively low flux of reactor neutrons does not affect the kinetics of fluid-solid adsorption, an additional *in-situ* SANS experiment was conducted at ambient conditions on the 0.5–1.0 mm particles of Mar-2, the clay-rich sample, to probe the kinetics of adsorption by the sample to water and toluene. For this kinetics experiment, scattering profiles were collected immediately after the contrast match solution of H₂O/D₂O and toluene/d-toluene was added to the Mar-2 powder samples. Note that *in-situ* experiments were carried out on non-saturated samples, whereas CM-SANS measurements were carried out after the samples were saturated for 1 hour with the fluid (water or toluene).

4. Results and Discussion:

4.1. SANS and microstructure of the Marcellus Shale – dry samples

Figure 3 shows the SANS profiles of the dry shale samples. The small-Q data show power law scattering behaviour – the scattering intensity varies as \sim Q^{- α} due to the surface fractal nature of the pore-matrix interface. The surface fractal dimension D_s, which can be obtained from the exponent α using the relationship α =6-D_s, varies between 2 and 3 for the three samples (Table 3). For a very smooth surface the fractal dimension is close to 2, for a very rough surface the fractal dimension is close to 3. For all three samples the data show a deviation from power law scattering as SANS intensity in the large-Q region is dominated by micropores (<2.5 nm) that are non-fractal in nature. Thus, the SANS data were analysed using the power law scattering, i.e. surface fractal model to account for the small-Q data and the polydisperse sphere model to account for the large-Q non-fractal scattering due to the presence of micropores. However, the spherical shape is only an approximation reflecting the average grain orientation within the powdered samples. The scattering intensity from the Marcellus Shale samples can be expressed

by adding fractal (Bale and Schmidt, 1984) and non-fractal scattering contributions as shown below (Bahadur et al., 2014):

216
$$I(Q) = CQ^{-\alpha} + n(\rho_{matrix} - \rho_{pore})^2 \int V_p^2(r)D(r)P(Q,r)dr + Bkg$$
 (eq 1)

217

218

219

220

221

222

223

224

225

226

227

228

229

230

231

232

233

234

235

where C is independent of Q (but depends on the contrast factor between grains and the voids within the sample) and Bkg is a flat (Q-independent) background arising from incoherent scattering from any hydrogen present and possibly heterogeneities on a size scale of <1 nm radius (Bahadur et al., 2015b). The middle terms in eq. 1 account for the contribution from the nanometre size pores present in the shale where n is the number density of pores, $(\rho_{\text{matrix}} - \rho_{\text{pore}})^2$ is a contrast factor (square of the SLD between the matrix and the nanometre size pores), P(q, r) is the form factor for spherical pores with radius r, V_p(r) is the volume of the spherical pore with radius r, and D(r) is the pore size distribution. Because it has been shown by theoretical calculations that nanometre size pores in shale possess a lognormal distribution (Cui and Cheng, 2017; Wang et al., 2015) we have assumed a lognormal distribution for the pores in the Marcellus Shale. In addition, the lognormal distribution is widely used in the analysis of smallangle scattering data on various materials (Bahadur et al., 2008; Beaucage et al., 2004; Lee et al., 2005). The fitting of the fractal as well as non-fractal scattering contributions for the three dry shale samples is shown in Fig. S1 (Supporting Information). The fitting of the model (eq.1) to the data and estimated pore size distributions are shown Fig. 3. Recently, it has been found that a portion of the total scattering could be induced from heterogeneities within the organic material, specifically nanometre-size mineral particles (Mares et al., 2012, Larichey et al., 2017, Radlinski and Mastalerz, this volume). The presence of nanometre size mineral inclusions may lead to the overestimation of pore number density shown on Table 3. See Sect. 4.2 for further discussion.

The contrast matching SANS can differentiate between mineral matter and nanometre sized pores in the organic matter if all pores are accessible.

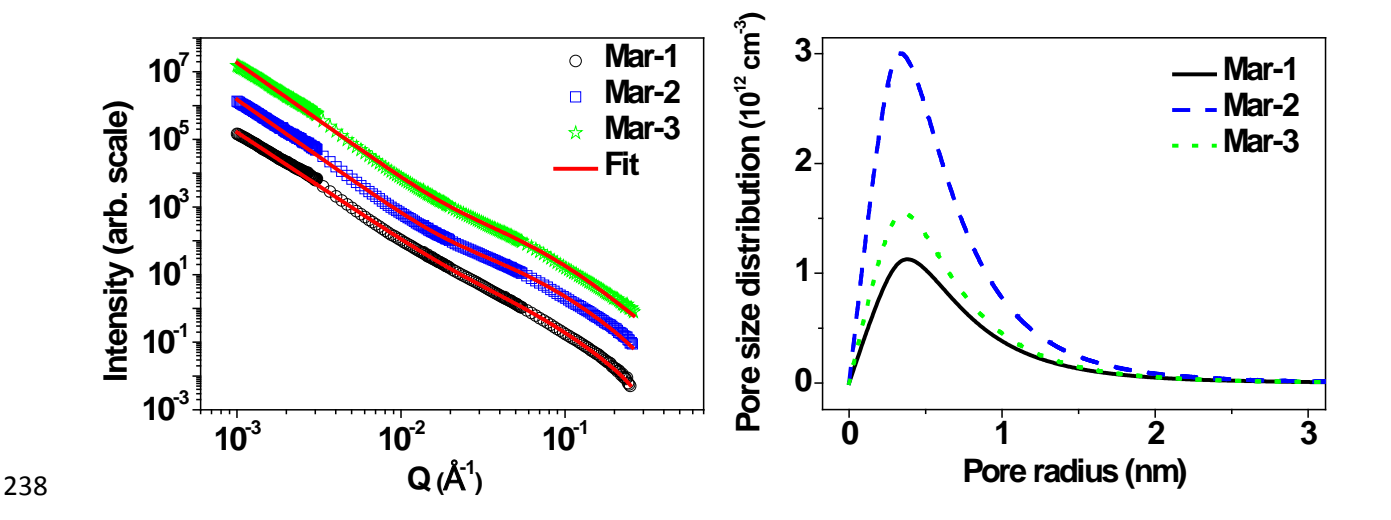


Fig. 3. (Left) Scaled scattering profiles of dry Marcellus Shale samples, corrected for background. The red line plots represent model fits to the data. (Right) The estimated pore size number distribution of the Marcellus Shale samples.

Table 3 *The parameters of model (eq. 1) obtained by fitting of the experimental data.*

Sample	Surface fractal dimension (D _s)	Number density of pores (cm ⁻³)	Average pore radius (nm)	Standard deviation (nm)
Mar-1	2.82	9.2 ×10 ¹²	0.75	0.54
Mar-2	2.62	2.1×10^{13}	0.67	0.48
Mar-3	2.60	1.18×10 ¹³	0.70	0.51

The fractal dimension for Mar-1 is significantly greater $(2.82 D_s)$ than the fractal dimensions of Mar-2 $(2.62 D_s)$ and Mar-3 $(2.60 D_s)$ samples (Table 3) which suggests that the differences in mineralogy may affect the structure of pore and grain interfaces within the samples. Interestingly, the average size of the pores is approximately the same in all three samples (0.67-

248 0.75 nm), but the number density of pores is highest in the Mar-2 (2.1×10^{13} cm⁻³) and lowest in the Mar-1 (9.2×10^{12} cm⁻³) sample.

4.2. Contrast matching SANS and microstructure

- To compare the ability of water and toluene to penetrate pores (which can be considered to be a proxy for wettability), SANS experiments were carried out on individual sub-splits of the three samples after a one hour immersion in H₂O/D₂O and toluene/d-toluene mixtures. Table S1 and Fig. 2 show the SLDs of H₂O/D₂O and toluene/d-toluene mixtures obtained by varying the volume ratio of H₂O and D₂O and toluene and d-toluene, respectively.
- The SANS profiles, corrected for the scattering from hydrogen in water and toluene, of the samples for different SLD mixtures of H₂O/D₂O and toluene/d-toluene are shown in Fig. S2 and Fig. S3 (Supporting Information).
- 259 For a fixed Q the scattering intensity can be written as:

260
$$I_{Qf}=K(\rho_{p}-\rho_{m})^{2}$$
 (eq 2)

where K is a constant and ρ_P , ρ_m are the SLDs of the pore and matrix, respectively. The SLD of accessible pores becomes equal to SLD of the penetrating liquid. It is evident from eq.2 that intensity at fixed Q is a parabolic function of ρ_P . The SLD of liquid corresponding to the minimum value of the intensity gives the SLD value of the matrix. The residual minimum scattering intensity provides information about fraction of inaccessible pores. Figure 4 shows the relationship between normalized scattering intensity at an arbitrarily selected Q (Q=0.1 Å⁻¹) and the SLD of the added liquid. It is observed that scattering intensity from the samples initially decreases with increasing amounts of deuterated solvent in the mixture, and then increases again,

in a parabolic fashion. The intensity of the dry samples is not shown on Fig. 4 as their addition extends the y-scale and obscures the parabolic behaviour. It is evident from figure that penetrating abilities of water and toluene are different in the three samples; not only are the minimum scattering intensities different, but the contrast matching SLD of shale obtained using toluene/d-toluene is higher than the contrast matching SLD obtained by H₂O/D₂O (Table 4).

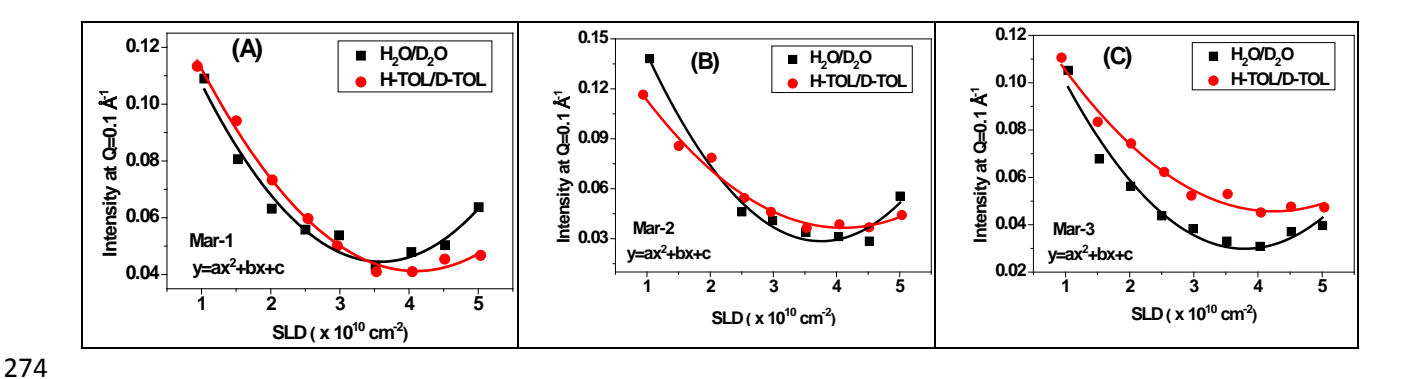


Fig. 4 Scattering intensity at $Q=0.1\text{Å}^{-1}$ for (A) Mar-1, (B) Mar-2 and (C) Mar-3 as a function of the scattering length density (SLD) of H_2O/D_2O and toluene/d-toluene (H-TOL/D-TOL) mixtures. The solid lines represent the polynomial (order-2) fit of the data. Note y-axis scale differences. The scattering intensity was normalized with the dry sample scattering.

Fitting of the experimental data using eq. 2 can also provide a rough estimate of the random error introduced during our sample preparation (hand-packing of powdered samples into the cuvettes). Figure 4 suggests that the packing repeatability was better than $\pm 15\%$. This estimate is within the packing variation estimated by the sample weight of a paired contrast matched sample ($\sim+8\%$).

Table 4 The scattering length density (SLD) obtained by contrast matching with H_2O/D_2O $[(\rho_m)_{Water}]$ and toluene/d-toluene $[(\rho_m)_{Toluene}]$ versus the SLD calculated $[(\rho_m)_{cal})]$ for each sample.

Sample	(pm)Water	$(\rho_m)_{Toluene}$	(ρ _m) _{Cal}	
	(10 ¹⁰ cm ⁻²)	(10 ¹⁰ cm ⁻²)	(10 ¹⁰ cm ⁻²)	
Mar-1	3.59±0.65	4.10±0.46	4.01	
Mar-2	3.75±0.69	4.10±0.78	3.99	
Mar-3	3.79±0.90	4.24±0.92	4.18	

As stated previously, the ratio of scatting intensity of the dry and contrast matched sample provides the fraction of accessible pores (Radlinski et al., 2000).

294
$$\frac{I(Q_i,CM)}{I(Q_i,dry)} = 1 - \eta_{ac}(Q_i)$$
 (4)

where $I(Q_i,CM)$, $I(Q_i,dry)$ are the scattering intensity of the contrast matched and dry shale samples at $Q=Q_i$, and η_{ac} is the volume fraction of accessible pores corresponding to that value of scattering vector. The volume fraction of accessible pores has been estimated using eq. 4 for the Marcellus Shale samples contrast matched with water and toluene are shown in Fig. 5.

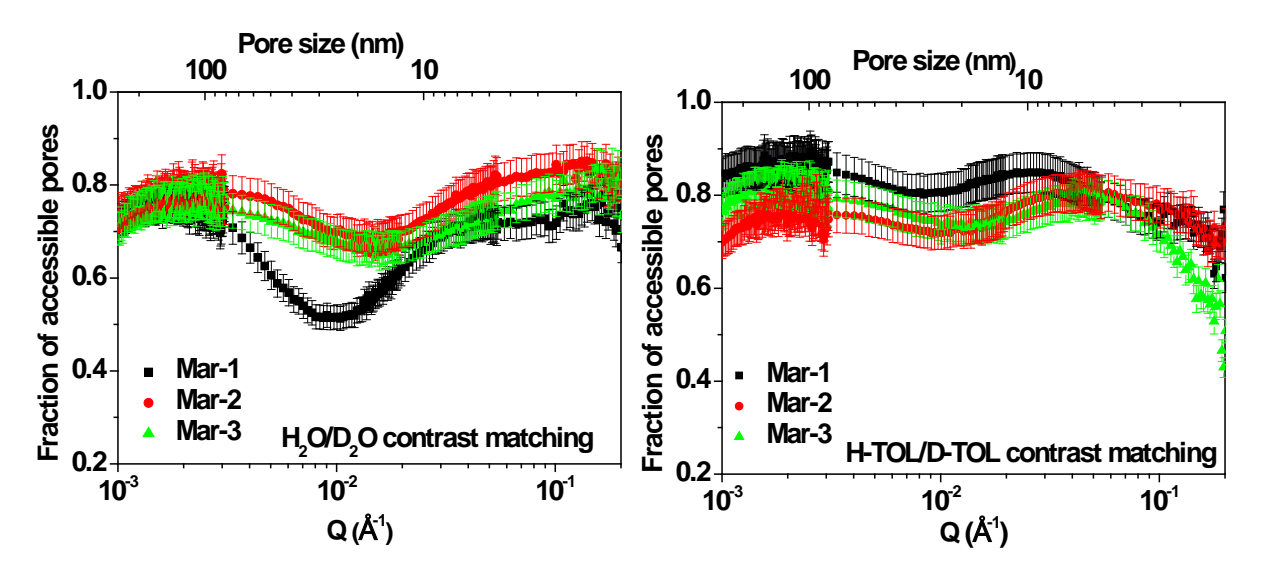


Fig. 5 The fraction of accessible pores in three Marcellus Shale samples estimated by: (left) H_2O/D_2O contrast matching and (right) toluene/d-toluene (H-TOL/D-TOL) contrast matching.

300

301

302

303

304

305

306

307

308

309

310

311

312

313

314

315

316

It is evident that accessibility of pores with water and toluene varies with pore size (fig. 5,6) and that the three samples show similar trends in their pore volume accessibility. In general, water accesses approximately 70-80% of the larger pores (>80 nm radius) in all three samples, but as pore size decreases (~5-80 nm radius) the fraction of accessible pores decreases with the quartzrich sample (Mar 1, fig. 5) exhibiting much lower accessibility than the clay- and carbonate-rich samples. At even smaller pore sizes (<2.5 nm radius) in all samples, the fraction of accessible pores to water increases to approximately 70–80%. Accessibility to toluene generally follows that of water, although it penetrates slightly more effectively than water into pores at Q<0.1 Å⁻¹ (>2.5 nm radius; figs. 5,6). However, at Q>0.1 Å⁻¹ (<2.5 nm radius; fig 5), pore accessibility to toluene decreases compared to that of water in all three samples with the carbonate-rich sample (Mar-3) showing the most dramatic decrease. The decrease at Q>0.1 Å⁻¹ may be related to an abundance of closed pores or simply that the toluene molecule is too large (kinetic diameter~6.7 Å) to fit into the throats of the smallest pores. To fully understand why the carbonate-rich sample shows such a dramatic decrease in toluene accessibility at large Q (in the micropore region) will require additional study, but it is probably not related to carbonate dissolution nor the higher

TOC content of the sample (9.60 wt.%, Table 2) as carbonates are insoluble in toluene at ambient conditions and this behaviour was not observed over the entire Q range.

317

318

319

320

321

322

323

324

325

326

327

328

329

330

331

332

333

334

335

The lowest accessibility to both fluids is at pore sizes of ~25 nm radius: Mar-1 shows the lowest accessibility to water and a lower accessibility to toluene around this pore size. The mechanism for this behaviour needs further study but it is probably not related to the presence of abundant quartz in Mar-1 as all three samples contain varying amounts of it (37–66 wt.%, Table 2). Because the mineralogy of the three samples varies, it is likely that the inaccessible ~25 nm radius pores are associated with organics and not a specific mineral within the samples (Table 2). Although both toluene and water penetrate most of the pores in the Marcellus Shale samples, even ones <2.5 nm in radius, there are differences in the extent to which the two fluids penetrate. Most of the minerals in the samples are intrinsically water-wet, and because water is a smaller molecule than toluene, we anticipated that water would access more of the pores than toluene. However, in these samples, toluene penetrates the ~2.5–250 nm radius pores better than water which suggests that pore and the mineral surfaces within the samples are likely predominately mixed-wet. During the Early Pennsylvanian oil window (Rowan et al., 2007), oil, or thin hydrophobic coatings, likely coated material and pore surfaces causing them to become mixedwet. If thin hydrophobic films are present in the Marcellus Shale (and we have no direct evidence for their presence or extractability), it may be possible to extract them with solvents, thus opening up gas-filled porosity and increasing natural gas production.

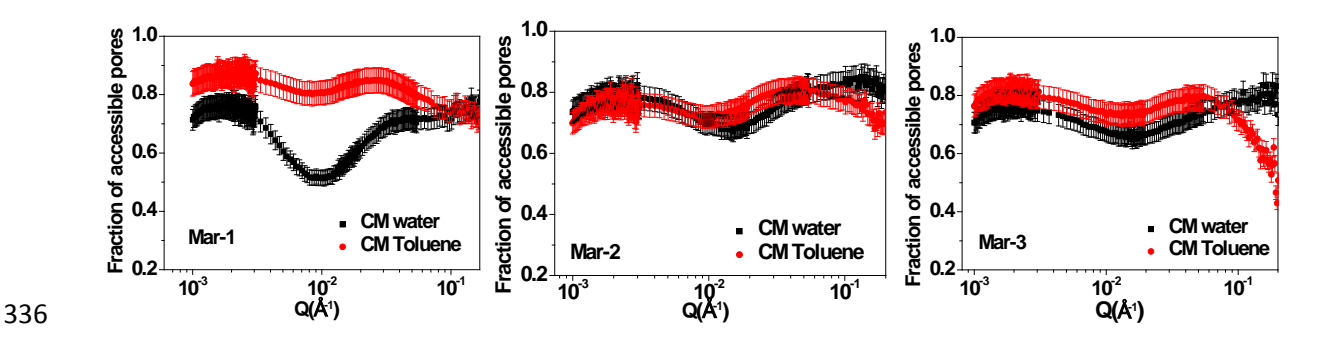


Fig. 6 Comparison of fractions of accessible pores estimated by H_2O/D_2O and toluene/d-toluene (H-TOL/D-TOL) contrast in (left) Mar-1, (middle) Mar-2 and (right) Mar-3. CM = contrast matching.

3.4. Kinetics for wetting process of shale with water and toluene

In-situ SANS wetting experiments were conducted under ambient conditions on two representative sub-splits of the 0.5–10 mm powders of Mar-2 (the clay-rich sample) to probe the adsorption kinetics of water and toluene in the Marcellus Shale. The H₂O/D₂O mixture used for the kinetic experiment had an SLD of 3.52 (Table S1, mixture W6): SLD of the toluene/d-toluene mixture was 4.04 (Table S1, mixture T7). These mixtures were chosen because their SLD was closest to the sample SLD obtained by contrast matching (Table 4). The water and toluene kinetics experiments were conducted for 440 minutes and 580 minutes, respectively. The first scattering intensities were measured immediately after the addition of the fluids and measurements continued overnight in one minute intervals. The H₂O/D₂O and toluene/d-toluene contrast matching scattering profiles as a function of time are shown in Supporting Information (fig. S4).

Figure 7 shows the normalized scattering intensity at Q=0.0005 Å⁻¹ and 0.001 Å⁻¹ and the integrated intensity as a function of time for H_2O/D_2O and toluene/d-toluene. These Q values were chosen because integrated scattering intensity is most strongly influenced by the measurements at low Q (~Q=0.0002 Å⁻¹).

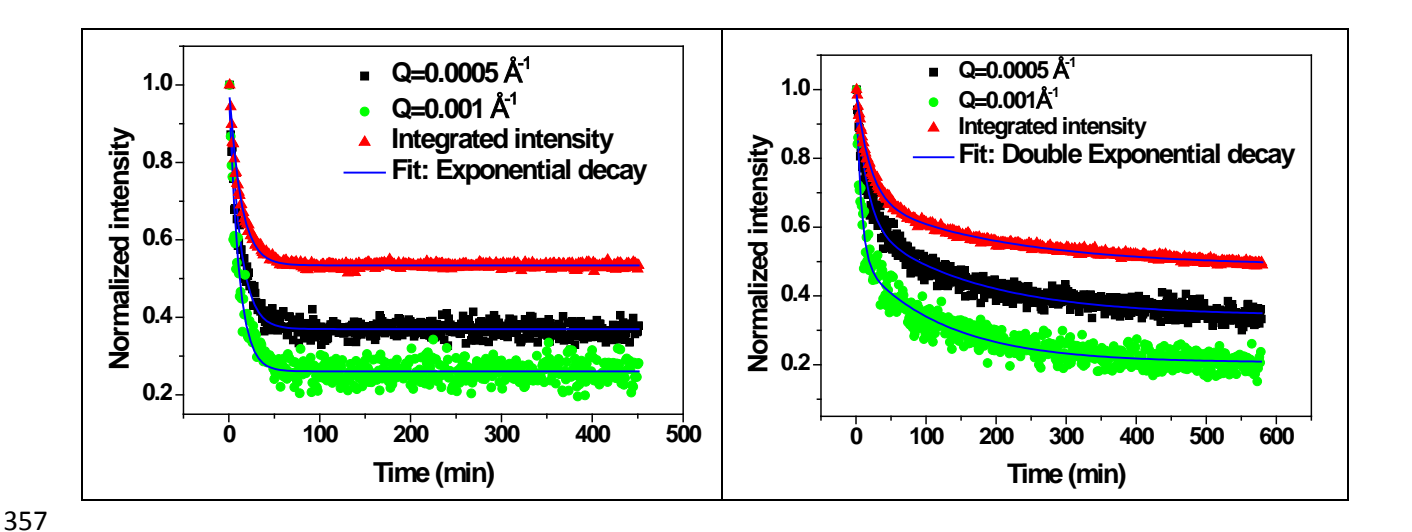


Fig. 7 Normalized scattering intensity at $Q=0.0005 \text{ Å}^{-1}$ and $Q=0.001 \text{ Å}^{-1}$ and integrated intensity as a function of time for water (left) and toluene (right), for sample Mar-2. Arb.= arbitrary.

The water data can be fitted with the single decay exponential function

$$361 y = 1 - A \left[1 - \exp\left(-\frac{t}{\tau}\right) \right] (5)$$

where A is the fraction of accessible pores, and ?? is the time constant of the decay of the intensity. Table 5 shows the fitting of the model (eq.5) to the water data.

Table 5: Single decay exponential function fitting parameters for H₂O/D₂O kinetics. A=the fraction of accessible pores; ??=time constant of decay, in minutes.

Length scales	A	?? (min)
$Q=0.0005 \text{ Å}^{-1} (500 \text{ nm})$	0.63±0.01	12.24±0.21
Q=0.001 Å ⁻¹ (250 nm)	0.739±0.01	10.55±0.25
Integrated intensity (0.5-350 nm)	0.465±0.004	13.07±0.10

The water penetration time constants are similar at both Q values and for integrated scattering intensity (Table 5). At Q=0.0005 Å^{-1} and Q=0.001 Å^{-1} the rate of penetration by water into

accessible pores is not affected by pore size. The single exponential fit also suggests that water does not change the pore structure of the sample, at least on the timescale of the test.

In contrast, the toluene penetration kinetics data are not fitted by a single decay exponential function: they must be fitted with a double decay exponential function that can be written as

373
$$y = 1 - A_s \left[1 - exp\left(-\frac{t}{\tau_s} \right) \right] \pm A_f \left[1 - exp\left(-\frac{t}{\tau_f} \right) \right]$$
 (6)

Table 6 shows the fitting of the model (eq.6) to the toluene kinetics data.

Table 6. Double decay exponential function fitting parameters for kinetics of toluene penetration into Mar-2. A_s =fractional contribution by slow component; τ_s =time constant associated with slow component; A_f =fractional contribution of fast component; τ_f =time constant associated with fast component.

Length scales	A_s	?? _s (min)	$\mathbf{A_f}$?? _f (min)
Q=0.0005 Å ⁻¹ (500 nm)	0.27±0.01	159±8	0.38±0.01	15.0±.7
Q=0.001 Å ⁻¹ (250 nm)	0.30±0.01	123±6	0.49±0.01	7.1±0.4
Integrated intensity (0.5–350 nm)	0.19±0.01	199±6	0.31±0.01	19.5±0.3

The time constant for the faster process (??f) is ~7–20 minutes (Table 6), comparable to the water penetration time constant. Its contribution to the total adsorption is greater at lower Q values. The time constant for the slower process (??s) is ~120–200 minutes (Table 6). The double decay exponential function fitting suggests that there are two separate processes occurring as toluene penetrate the pores in this sample. Figure 7 shows that water is sorbed in pores more rapidly than toluene; results also suggest that toluene will continue to penetrate more pores over time (Fig. 8).

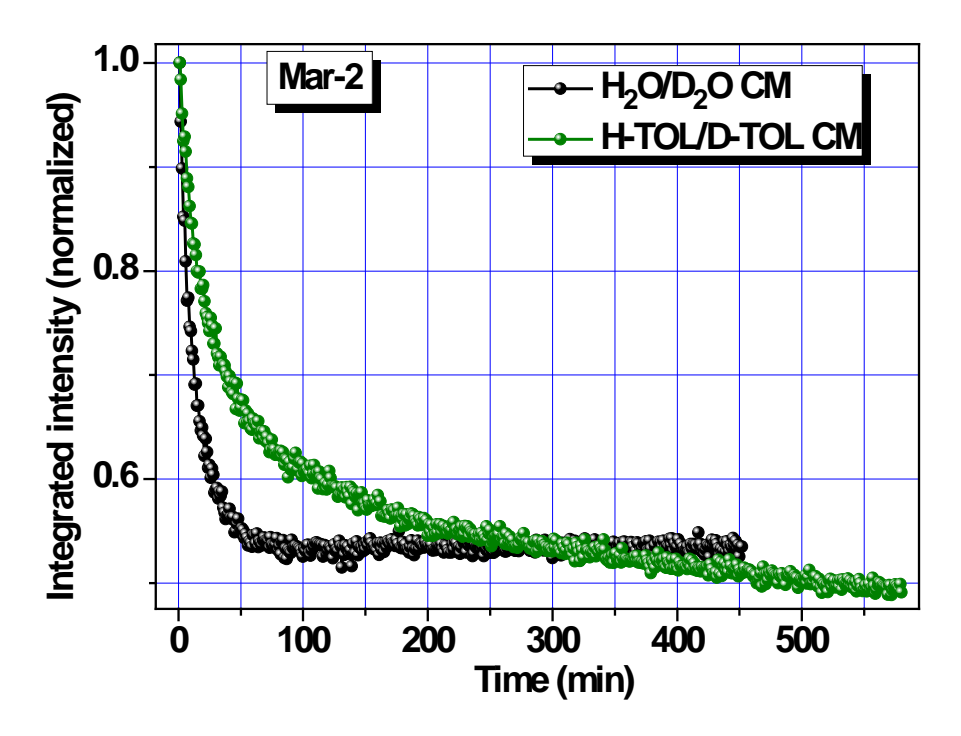


Fig. 8 - The evolution of integrated intensity with time showing kinetics of the water (H₂O/D₂O) and toluene (H-TOL/D-TOL) penetration in Mar-2, the clay-rich sample. CM=contrast matching.

There are several possible explanations for the slow rate constant for toluene, including i) toluene modifies the structure of the organic material associated with the pores and mineral matter, but the process is slow (>125 minutes); ii) toluene slowly displaces any bound water within the sample; and iii) the large size of the toluene molecule delays penetration into the pores. Clearly, further work is required to understand the slow rate constant of toluene as the kinetics data suggest that longer exposure times are necessary for toluene to fully equilibrate with the shale.

4. Conclusions

Three Middle Devonian Marcellus Shale samples, representing quartz-rich, clay-rich, and carbonate-rich facies, were examined using neutron scattering techniques to determine the effect

of mineral matter on the accessibility of water and toluene to pores of 1.0–250 nm radii within the shale matrix.

- 1. The fractal dimension for the quartz-rich sample was higher than for the clay-rich and carbonate-rich samples suggesting that there are differences in both the mineralogy and the structure of pore and grain interfaces between the samples.
- 2. At Q>0.1 Å⁻¹ (pore radius >2.5–250 nm), most of the pores are largely penetrable by both water and toluene in all three samples. At Q=0.1 Å⁻¹, toluene accessibility decreases which may indicate increased numbers of closed micropores or simply that the toluene molecule (6.7 Å) is too large to fit into the smallest pores.
- 3. The extent of pore penetration with both water and toluene reaches a minimum at around Q=0.01 Å⁻¹ (~25 nm) suggesting that there are more closed pore structures around this size range or there is greater heterogeneity, compared to other size ranges.
- 4. There are differences in the SLD values at which toluene and water reach a minimum scattering intensity suggesting that water and toluene penetrate, or wet, different parts of the shale matrix or different pore size ranges. Water appears to be more selective in its wettability of pores than toluene as its contrast matching SLD is smaller than the average measured SLD for the shale samples: water avoids and does not wet high SLD components. This finding suggests that mineralogic variations may account for some of the differences in hydrocarbon production and recovery observed within a reservoir.
- 5. The kinetics of penetration by water can be modelled by a single exponential fit. The kinetics of penetration by toluene requires a two-component exponential fit and shows that there is a slow adsorption step with a time constant of ~120-200 min.

Acknowledgements

424

- 425 This research was supported in part by the ORNL Postdoctoral Research Associates Program,
- administered jointly by the ORNL and the Oak Ridge Institute for Science and Education. This
- work is based upon experiments performed at the KWS-1 and KWS-3 instruments operated by
- Dr. Vitaliy Pipich at the Heinz Maier-Leibnitz Zentrum (MLZ), Garching, Germany. Use of
- 429 trade, product, or firm names is for descriptive purposes only and does not imply endorsement by
- 430 the U.S. Government.

431 References

- 432 Abdullah, W., Buckley, J.S., Carnegie, A., Edwards, J., Fordham, E., Graue, A., Habashy, T., Seleznev, N.,
- Signer, C., Hussain, H., Montaron, B., Ziauddin, M., 2007. Fundamentals of wettability. Oilfield Review,
- 434 44-61.
- 435 Bahadur, J., Melnichenko, Y., Mastalerz, M., Furmann, A., Clarkson, C.R., 2014. Hierarchical pore
- 436 morphology of cretaceous shale: a small-angle neutron scattering and ultrasmall-angle neutron
- 437 scattering study. Energy Fuels. 28, 6336-6344.
- 438 Bahadur, J., Melnichenko, Y.B., He, L., Contescu, C.I., Gallego, N.C., Carmichael, J.R., 2015a. SANS
- 439 investigations of CO₂ adsorption in microporous carbon. Carbon. 95, 535-544.
- 8440 Bahadur, J., Radlinski, A.P., Melnichenko, Y.B., Mastalerz, M., Schimmelmann, A., 2015b. Small-angle and
- 441 ultrasmall-angle neutron scattering (SANS/USANS) study of New Albany shale: a treatise on
- 442 microporosity. Energy Fuels. 29, 567-576.
- 443 Bahadur, J., Sen, D., Mazunder, S., Shukla, R., Tyagi, A.K., 2008. Non-Debye to Debye transition of ac
- dielectric response in YCrO₃ nanoceramic under sintering: effect of pore structure. J. Phys.: Condens.
- 445 Matter. 20, 345201.
- 446 Bale, H.D., Schmidt, P.W., 1984. Small-Angle X-Ray-Scattering Investigation of Submicroscopic Porosity
- with Fractal Properties. Phys. Rev. Lett. 53
- 448 Beaucage, G., Kammler, H.K., Pratsinis, S.E., 2004. Particle size distributions from small-angle scattering
- using global scattering functions. J. Appl. Cryst. 37, 523-535.
- 450 Blach, T., Radlinski, A.P., Edwards, D.S., Boreham, C.J., Rehm, C., de Campo, L., Gilbert, E.P., Fingerprint
- 451 of hydrocarbon generation in the southern Georgina Basin, Australia, revealed by small angle neutron
- 452 scattering. Inter. J.Coal Geol. This volume.
- 453 Brumberger, H., Goodisman, J., 1983. Voronoi cells: an interesting and potentially useful cell model for
- interpreting the small-angle scattering of catalysts. J. Appl. Cryst. 16, 83-88.
- Busch, A., Gensterblum, Y., 2011. BM and CO₂-ECBM related sorption processes in coal: A review. Int. J.
- 456 Coal Geol. 87, 49-71.

- 457 Clarkson, C.R., Freeman, M., He, L., Agamalian, M., Melnichenko, Y.B., Mastalerz, M., Bustin, R.M.,
- 458 Radliński, A.P., Blach, T.P., 2012. Characterization of tight gas reservoir pore structure using
- 459 USANS/SANS and gas adsorption analysis. Fuel. 95, 371-385.
- 460 Clarkson, C.R., Solano, N., Bustin, R.M., Bustin, A.M.M., Chalmers, G.R.L., He, L., Y.B. Melnichenko,
- Radliński, A.P., Blach, T.P., 2013. Pore structure characterization of North American shale gas reservoirs
- using USANS/SANS, gas adsorption, and mercury intrusion. Fuel. 103, 606-613.
- 463 Coetzee, H., Sakurovs, R., Neomagus, H., Morpeth, L., Everson, R.C., Mathews, J.P., Bunta, J.R., 2015.
- 464 Pore development during gasification of South African inertinite-rich chars evaluated using small angle
- 465 X-ray scattering. Carbon. 95, 250-260.
- 466 Cui, J., Cheng, L., 2017. A theoretical study of the occurrence state of shale oil based on the pore sizes of
- 467 mixed Gaussian distribution. Fuel. 206, 564-571.
- 468 Foster M.D, Jensen K.F., 1990. Interpreting scattering from random porous solids: A model of fully
- penetrable spherical voids. J. Colloid Interf. Sci. 135, 132-146.
- 470 Furmann, A., Mastalerz, M., Schimmelmann, A., Pedersen, P.K., Bish, D., 2014. Relationships between
- 471 porosity, organic matter, and mineral matter in mature organic-rich marine mudstones of the Belle
- 472 Fourche and Second White Specks formations in Alberta. Canada. Mar. Pet. Geol. 54, 65-81.
- 473 Gao, Z., Hu, Q., 2015. Wettability of Mississippian Barnett Shale samples at different depths:
- 474 Investigations from directional spontaneous imbibition. AAPG Bull. 100, 01-114.
- 475 Gu, X., Cole, D.R., Rother, G., Mildner, D.F.R., Brantley, S.L., 2015. Pores in Marcellus Shale: A Neutron
- 476 Scattering and FIB-SEM Study. Energy Fuels. 29, 1295-1308.
- 477 Gu, X., Mildner, D.F.R., Cole, D.R., 2016. Quantification of organic porosity and water accessibility in
- 478 Marcellus Shale using neutron scattering. Energy Fuels. 30, 4438-4449.
- Hall, P.J., Ruiz, M.W., Gascon, G., D., Barria, E.B., Sherrington, D.C., 1996. Use of contrast matching
- 480 small-angle neutron scattering to monitor the presence of closed porosity in controlled porosity
- 481 styrene–divinylbenzene resins. J. Chem. Soc., Faraday Trans. 92, 2607-2610.
- 482 Heinz Maier-Leibnitz Zentrum 2015a. KWS-1: Small-angle scattering diffractometer. Journal of Large-
- scale Research Facilities. 1, A28. http://dx.doi.org/10.17815/jlsrf-1-26.
- 484 Heinz Maier-Leibnitz Zentrum 2015b. KWS-3: Very small angle scattering diffractometer with focusing
- 485 mirror. Journal of Large-scale Research Facilities. 1, 31. http://dx.doi.org/10.17815/jlsrf-1-28.
- 486 He, L., Melnichenko, Y.B., Mastalerz, M., Sakurovs, R., Radlinski, A.P., Blach, T., 2012. Pore accessibility
- by methane and carbon dioxide in coal as determined by neutron scattering. Energy Fuels. 26, 1975-
- 488 1983.
- 489 Hosterman, J.W., Dulong, F.T., 1989. A computer program for semiquantitative mineral analysis by X-ray
- 490 powder diffraction, in: Pevear, D.A., Mumpton, F.A. (Eds.), Quantitative mineral analysis of clays:
- 491 Bloomington, Indiana. CMS Workshop Lectures. 37-50.
- 492 Larichev, Y.T., Szhogina, A.A., Bairamukov, Y.U., 2017. Small angle neutron and X-ray studies of carbon
- structures with metal atoms. IOP Conf. Series: Journal of Physics: Conf. Series 848.
- 494 László, K., Czakkel, O., Demé, B., Geissler, E., 2012. Simultaneous adsorption of toluene and water vapor
- on a high surface area carbon. Carbon. 50, 4155-4162.
- 496 Lee, B., Park, Y.-H., Hwang, Y.-T., Oh, W., Yoon, J., Ree, M., 2005. Ultralow-k nanoporous organosilicate
- 497 dielectric films imprinted with dendritic spheres. Nature Materials. 4, 147-150.

- 498 Mares, T.E., Radliński, A.P., Moore, T.A., Cookson, D., Thiyagarajan, P., Ilavsky, J., Klepp, J., 2012.
- 499 Location and distribution of inorganic material in a low ash yield, subbituminous coal. Inter. J. Coal Geol.
- 500 94173-181.
- 501 Mastalerz, M., He, L., Melnichenko, Y.B., Rupp, J.A., 2012. Porosity of coal and shale: Insights from gas
- adsorption and SANS/USANS techniques. Energy Fuels. 26, 5109-5120.
- 503 Melnichenko, Y.B., 2016. Small-Angle Neutron Scattering from Confined and Interfacial Fluids. Springer
- New York.
- Melnichenko, Y.B., He, L., Sakurovs, R., Kholodenko, A.L., Blach, T., Mastalerz, M., Radliński, A.P., Cheng,
- 506 G., Mildner, D.F.R., 2012. Accessibility of pores in coal to methane and carbon dioxide. Fuel. 91, 200-208.
- 507 Milici, R.C., Swezey, C.S., 2014. Assessment of Appalachian basin oil and gas resources; Devonian gas
- shales of the Devonian Shale-Middle and Upper Paleozoic Total Petroleum System, in: Ruppert, L.F.,
- 509 Ryder, R.T. (Eds.), Coal and petroleum resources in the Appalachian basin; Distribution, geologic
- framework, and geochemical character. USGS Prof. Paper 1708, p. 81.
- Radlinski, A.P., 2006. Small-angle neutron scattering and the microstructure of rocks. Reviews in Min.
- 512 Geochem. 63, 363-397.
- 513 Radlinski, A.P., Boreham, C.J., Lindner, P., Randl, O., Wignall, G.D., Hinde, A., Hope, J.M., 2000. Small
- angle neutron scattering signature of oil generation in artificially and naturally matured hydrocarbon
- 515 source rocks. Org. Geochem. 31, 1-14.
- 516 Radlinski, A.P., Mastalerz, M., Neutron scattering study of vitrinite: Insights into sub-micrometer
- 517 inclusions in North American Carboniferous coals of bituminous rank. Inter. J. Coal Geol. This volume.
- Radlinski, A.P., Mastalerz, M., Hinde, A.L., Hainbuchner, M., Rauch, H., Baron, M., Lin, J.S., Fan, L.,
- 519 Thiyagarajan, P., 2004. Application of SAXS and SANS in evaluation of porosity, pore size distribution and
- surface area of coal. Inter. J. Coal Geol. 59, 245-271.
- Ruppert, L., Sakurovs, R., Blach, T.P., He, L., Melnichenko, Y.B., Mildner, D.F., Alcantar-Lopez, L., 2013. A
- 522 USANS/SANS study of the accessibility of pores in the Barnett shale to methane and water. Energy Fuels.
- 523 27, 772-779.
- 524 Sakurovs, R., He, L., Melnichenko, Y.B., Radlinski, A.P., Blach, T., Lemmel, H., Mildner, D.F.R., 2012. Pore
- size distribution and accessible pore size distribution in bituminous coals. Inter. J. Coal Geol. 100, 51-64.
- 526 Sakurovs, R., Koval, L., Grigore, M., Sokolova, A., Ruppert, L.F., Melnichenko, Y.B., Nanometre-sized
- 527 pores in coal: Variations between coal basins and coal origin. Inter. J. Coal Geol. This volume.
- 528 Soeder, D.J., Enomoto, C.E., Chermak, J.A., Shale., T.D.M.S.a.M., 2014. The Devonian Marcellus Shale
- and Millboro Shale, Geol. Soc. Amer. Field Trip Guide #5.
- 530 Staib, G., Gray, E., Sakurovs, R., Webb, J., 2013. Direct evidence of slow kinetics of CO2 and CH4
- 531 penetration into coals using small angle x-ray scattering experiments, in: Jonathan, M., Elizabeth, W.,
- 532 Shea, W. (Eds.), International Conference on Coal Science and Technology (ICCS&T), EMS Energy
- 533 Institute, Penn. State University. 1567-1584.
- U.S. Energy Information Administration 2012 Annual Energy Outlook 2012, DOE/EIA-0383.
- 535 http://www.nrc.gov/docs/ML1409/ML14093A265.pdf.
- 536 U.S. Energy Information Administration, 2017. Frequently asked questions. .
- 537 https://www.eia.gov/tools/faqs/faq.php?id=907&t=8.

- Utpalendu, K., McCarty, D.K., Derkowski, A., Fischer, T.B., Prasad, M., 2014. Total porosity measurement
- in gas shales by the water immersion porosimetry (WIP) method. Fuel. 117, 1115-1129.
- Wang, S., Feng, Q., Javadpour, F., Xia, T., Li, Z., 2015. Oil adsorption in shale nanopores and its effect on
- recoverable oil-in-place. Inter. J. Coal Geol. 147-148, 9-24.
- Xu, M., Dehghanpour, H., 2014. Advances in understanding wettability of gas shale. Energy Fuels. 28,
- 543 4362-4375.
- Zhang, R., Liu, S., Bahadur, J., Elsworth, D., Melnichenko, Y.B., He, L., Wang, Y., 2015. Estimation and
- modeling of coal pore accessibility using small angle neutron scattering. Fuel. 161, 323-332.